Nanoscale

PAPER

View Article Online
View Journal | View Issue

Cite this: *Nanoscale*, 2014, **6**, 1823

Plasmonic dye-sensitized solar cells incorporated with Au–TiO_2 nanostructures with tailored configurations†

Yoon Hee Jang,[a] Yu Jin Jang,[a] Saji Thomas Kochuveedu,[a] Myunghwan Byun,[c] Zhiqun Lin[b] and Dong Ha Kim*[a]

Received 18th September 2013
Accepted 20th November 2013

DOI: 10.1039/c3nr05012b

www.rsc.org/nanoscale

We developed plasmonic dye-sensitized solar cells (DSSCs) with tailor-designed Au–TiO_2 nanostructures integrated into the photoanode. Mutually antagonistic Au–TiO_2 core–shell structures supported on SiO_2 spheres (SiO_2@TiO_2@AuNP and SiO_2@AuNP@TiO_2) were prepared and incorporated as additives into the photoanodes of the DSSCs. The DSSCs employing the nanocrystalline-TiO_2 (nc-TiO_2)/SiO_2@TiO_2@AuNP and nc-TiO_2/SiO_2@AuNP@TiO_2 as photoanodes showed remarkably enhanced power conversion efficiencies up to about 14% and 10%, respectively, with respect to a reference cell containing an nc-TiO_2/SiO_2@TiO_2 photoanode. This can be mainly attributed to the enhanced dye absorption by the intensified near-field effect of AuNPs and plasmon-enhanced photocurrent generation.

Introduction

Noble metal nanoparticles (NPs) have widely been applied in various research fields, including optical sensors,[1–4] catalysts,[5,6] and surface-enhanced Raman scattering,[7–9] due to their characteristic optical and electrical properties, which are not available with bulk analogues. Particularly, the feature of localized surface plasmon resonance (LSPR), collective oscillations of the free conduction band electrons at the interface between the surface of metal NPs and dielectrics, has been attracting attention, because it can concentrate the optical fields of incident light when the wavevector matches between an incident photon and a surface plasmon.[10–13] On the basis of the LSPR effect, plasmonic nanostructures have been increasingly exploited to enhance the performance of photovoltaic devices, for which the mechanism has mainly been described to have a strong light scattering effect and local field enhancement.[14–20] Recently, many efforts have been devoted to increasing the light harvesting efficiency by introducing plasmonic structures into various types of solar cells. Derkacs *et al.* reported that an engineered enhancement in short-circuit current density and power conversion efficiency was achieved *via* forward scattering of the surface plasmon polariton modes in AuNPs deposited above amorphous Si solar cells.[21] The optical path length of the incident light in the absorber layers was increased by the strong scattering behaviour of the AgNPs in thin GaAs solar cells, resulting in an 8% increase in the current density, which was demonstrated by Nakayama *et al.*[22] You *et al.* demonstrated a highly efficient plasmonic polymer solar cell by introducing a metal-grating back-contact electrode. The resulting enhancement is attributed to local near-field enhancement, as well as the scattering effect.[23] Wang *et al.* added Ag clusters consisting of AgNPs with controlled diameter to the active layer of a bulk heterojunction solar cell, and improved photovoltaic parameters were obtained.[24] Standridge *et al.* examined the plasmon-enhanced optical absorption of the dye by adjusting the thickness of TiO_2 shell on AgNPs in dye-sensitized solar cells (DSSCs), thereby increasing the photocurrent.[25]

One of the important issues in plasmonic DSSCs is the stability of the NPs. When introduced metal NPs make direct contact with the iodide/triiodide-based liquid electrolyte, several problems arise, such as recombination, back reaction of the excited electrons, and the corrosion of NPs.[26–29] Core–shell NPs have recently been applied to address these issues (*e.g.*, metal@metal oxide core–shell structures).[30–33] Brown *et al.* reported plasmon-enhanced light absorption, photocurrent, and efficiency by incorporating Au@SiO_2 core–shell NPs into TiO_2 paste for both iodide/triiodide-electrolyte-based DSSCs and solid-state DSSCs.[34] Choi *et al.* investigated the effects derived from SiO_2-encapsulated and TiO_2-encapsulated AuNPs in DSSCs.

[a]*Department of Chemistry, Global Top 5 Research Program, Ewha Womans University, 52, Ewhayeodae-gil, Seodaemun-gu, Seoul, 120-750, South Korea. E-mail: dhkim@ewha.ac.kr; Fax: +82 2 3277 3419; Tel: +82 2 3277 4517*

[b]*School of Materials Science and Engineering, Georgia Institute of Technology, Atlanta, GA 30332, USA*

[c]*Department of Materials Science and Engineering, Korea Advanced Institute of Science and Technology, 291 Daehak-ro, Yuseong-gu, Daejeon, 305-701, South Korea*

† Electronic supplementary information (ESI) available: Additional data including SEM images of the SiO_2 spheres with different sizes, a summary of synthesis conditions of the SiO_2 spheres, TEM images and UV-Vis absorption spectra of the AuNPs, elementary mapping of the core–shell structures, SEM images of size-controlled SiO_2@TiO_2 core–shell structures, multiple linear-sweep voltammetry (LSV) curves of SiO_2@TiO_2@AuNP-containing TiO_2 films, and visible light-driven photocurrent response curves of SiO_2@TiO_2 and SiO_2@TiO_2@Au core–shell structures are available. See DOI: 10.1039/c3nr05012b

Plasmonic and electron charging effects were suggested to explain the higher photocurrent and increased photovoltage, respectively.[35] However, until now, there has been strong controversy regarding the role of plasmonic NPs in DSSCs, and more in-depth investigation for the enhancement mechanism is still required. In this study, in order to investigate the plasmonic effects and elucidate the working principle more systematically, we designed core–shell plasmonic nanostructures consisting of AuNP–TiO_2 supported on SiO_2 spheres, and incorporated them into a nanocrystalline-TiO_2 (nc-TiO_2)-based photoanode. We elaborate upon the architecture of the core–shell NPs by preparing mutually reverse configurations, AuNP@TiO_2 and TiO_2@AuNP, based on which better understanding of the contribution to the photovoltaic parameters can be attained.

Experimental

Synthesis of APTMS-SiO_2 spheres

Silica (SiO_2) spheres with various sizes were prepared according to the previously described modified Stöber method.[36] Tetraethyl orthosilicate (TEOS, 99%) was added as a precursor to a mixed solution consisting of de-ionized (DI) water, normal ethanol, and aqueous ammonia solutions (26%) under vigorous stirring at ambient temperature.[37] The detailed synthesis conditions are summarized in Table S1.† After 4 h, (3-aminopropyl)trimethoxysilane (APTMS, 100 μL) was added, and then the mixture was refluxed by maintaining a static temperature of 85 °C for 4 h. APTMS-treated SiO_2 spheres were centrifuged and washed with ethanol several times, and then the dried white powder was collected.

Synthesis of SiO_2@TiO_2 core–shell structures

To coat the TiO_2 shell on APTMS-modified SiO_2 spheres, as prepared APTMS-SiO_2 spheres (25 mg) were re-dispersed in ethanol (25 mL) by sonication and gentle stirring for 1 h. Appropriate amounts of titanium tetraisopropoxide (TTIP)/anhydrous ethanol solution (75 μL/7.5 mL) were dripped into SiO_2 ethanol solution using a syringe pump at a rate of 0.5 mL min^{-1}, and stirred for another 30 min after injection, followed by refluxing at 80 °C for 2 h without stirring. The resultant SiO_2@TiO_2 was centrifuged and washed with ethanol, and then dried.

Synthesis of SiO_2@TiO_2@AuNP core–shell structures

SiO_2@TiO_2@AuNP core–shell structures were prepared by incorporating the citrate-stabilized AuNPs. In a separate reaction, citrate-capped AuNPs of 15 nm size were synthesized with the method pioneered by Turkevich *et al.*[38] In order to decorate the AuNPs, SiO_2@TiO_2 was further modified by adding APTMS (16 μL) into dispersed SiO_2@TiO_2 in ethanol (25 mg mL^{-1}). APTMS-SiO_2@TiO_2 (25 mg) was dispersed well in citrate–Au aqueous solution (150 mL) and vigorously stirred for at least 4 h at room temperature. The final products of SiO_2@TiO_2@AuNP core–shell structures were obtained after washing with DI-water and drying.

Synthesis of SiO_2@AuNP@TiO_2 core–shell structures

For SiO_2@AuNP@TiO_2 core–shell structures, the above procedures were conducted in reverse. Shortly, APTMS-SiO_2 (25 mg) was dispersed in citrate–Au aqueous solution (150 mL) and stirred. Then, the obtained SiO_2@AuNP powder (25 mg) was re-dispersed in normal ethanol (25 mL), and APTMS (10 μL) was added. SiO_2@AuNP was covered with TiO_2 shell by adding TTIP and refluxing. The reddish SiO_2@AuNP@TiO_2 core–shell structures were finally obtained after the removal of unreacted TiO_2 precursors.

Fabrication of dye-sensitized solar cells

The nc-TiO_2 films with different types of core–shell structures added were utilized as photoanodes. Before use, fluorine-doped tin oxide (FTO, 2.2 mm thick and sheet resistance of 6–9 Ohms $sq.^{-1}$) glass pieces were washed by sonication in acetone, isopropanol, and DI water baths sequentially for 10 min. The nc-TiO_2/core–shell films were fabricated according to a previously reported process.[39] Briefly, a certain amount (0.3–5.0 wt%) of as-prepared core–shell structures was mixed with a TiO_2 paste (consisting of P25 TiO_2, ethyl cellulose, α-terpineol, and ethanol) and doctor-bladed onto the FTO glass substrate (the entire thickness of photoanodes is fixed at ~5 μm). The deposited films were heated at gradually increased temperatures, 125 °C, 325 °C, 375 °C, 450 °C, and 500 °C. Prior to dye adsorption, sintered nc-TiO_2/core–shell films were treated by $TiCl_4$ (40 mM) and exposed to oxygen plasma for 10 min under a given condition of 50 sccm (standard cubic centimeter per minute) and 100 W. Subsequently, nc-TiO_2/core–shell films were sensitized by the ruthenium dye (*cis*-diisothiocyanato-bis(2,2′-bipyridyl-4,4′-dicarboxylato) ruthenium (II) bis(tetrabutylammonium), N-719, Solaronix) by soaking in 0.2 mM dye–ethanol solution for 24 h. The nc-TiO_2/core–shell photoanodes and platinum counter electrodes (average thickness of Pt is ~2.8 nm) were assembled by insertion of a spacer (50 μm-thick hot-melt sealing foil, SX1170-25, Solaronix) and an ionic liquid electrolyte 0.60 M BMIM-I, 0.03 M I_2, 0.50 M TBP, and 0.10 M GTC in acetonitrile–valeronitrile 85/15 (v/v) (no. ES-0004), purchased from io.li.tec (Germany), was then injected into the small gap between two electrodes driven by capillary force. The photoactive area for DSSCs was 0.25 cm^2.

Characterization

Structures of core–shell nanocomposites were thoroughly examined by scanning electron microscopy (SEM, JEOL JSM6700-F, at 10 kV) and transmission electron microscopy (TEM, JEOL JSM2100-F, at 100 kV). Energy-dispersive X-ray (EDX) elementary mapping analysis was carried out using TEM equipment. The optical properties were measured by UV-Vis absorption spectroscopy (Cary 5000, Varian Inc.). Photocurrent–voltage curves were measured under a simulated 1.5 G illumination intensity of 100 mA cm^{-2} using a K3000 McScience Inc. measurement system. Photoelectrochemical measurement and photoelectrochemical (PEC) water splitting were performed in 0.1 M NaOH electrolyte using a potentiostat (Autolab PGSTAT302N, Eco Chemie). Three-electrode systems were used,

which contained nc-TiO_2/core–shell structures on an FTO substrate without dye as a working electrode, Ag/AgCl in 3 M KCl as a reference electrode, and platinum sheet as a counter electrode. The active area was 0.36 cm^2, and the scan rate was 10 mV s^{-1}. For PEC water splitting, SiO_2@TiO_2 and SiO_2@TiO_2@AuNP core–shell structures were mixed with a few drops of Nafion, and then they were applied on an indium tin oxide (ITO) substrate, followed by drying at 60 °C for 20 min. This is then used as the working electrode. Current-*versus*-potential curves were measured under visible light illumination using a 420 nm cut-off filter (Newport, 300 W Xe lamp) or 532 nm laser (OEM Laser System Inc.). The incident photon-to-current conversion efficiency (IPCE) was measured using a K3100 McScience Inc. measurement system with bias light.

Results and discussion

SiO_2 microspheres (mean diameter of around 200 nm, Fig. S1†) were prepared through the modified Stöber method, and consecutively treated by APTMS to introduce an amine group on the SiO_2 surface. The amine functionality facilitates the deposition of TiO_2 shells, or the anchoring of citrate-stabilized AuNPs through chemical affinity. Fig. 1 shows the electron microscope images of SiO_2@TiO_2, SiO_2@TiO_2@AuNP, and SiO_2@AuNP@TiO_2. As shown in Fig. 1a and d a thin layer of amorphous TiO_2 shell with a thickness of about 10–15 nm was uniformly coated onto amine-functionalized SiO_2 spheres by the sol–gel reaction and hydrolysis of TTIP in anhydrous ethanol. In contrast to the smooth surface of a bare SiO_2 core (Fig. S1†), the surface of the SiO_2@TiO_2 composite was rough. The surface of SiO_2@TiO_2 was treated with APTMS once more to induce Au anchoring sites.[40–42] After modification, citrate-capped AuNPs (about 15 nm in size, Fig. S2†) were evenly decorated without aggregation, and finally, a reddish powder of SiO_2@TiO_2@AuNP was obtained (Fig. 1b and e). Attached AuNPs were clearly observed outside the SiO_2@TiO_2. To prepare the SiO_2@AuNP@TiO_2 composite, the order of synthesis procedures was reversed: AuNPs were first decorated on SiO_2 and then the TiO_2 shell was applied. Fig. 1c and f clearly show that AuNPs are completely covered with a TiO_2 thin layer. Comparing the electron microscope images, the two types of core–shell structures, SiO_2@TiO_2@AuNP and SiO_2@AuNP@TiO_2 composites, were quite distinct from each other. The elementary compositions and formation of core–shell structures were also confirmed by EDX elementary mapping analysis (Fig. S3†). The overall fabrication process is depicted in Scheme 1, and the detailed synthesis process is explained in the Experimental section.

The normalized UV-Vis absorption spectra of the SiO_2, SiO_2@TiO_2, SiO_2@AuNP, SiO_2@TiO_2@AuNP, and SiO_2@AuNP@TiO_2 core–shell nanostructures are provided in Fig. 2. The strong absorption edge in the UV region (around 300 nm) comes from the intrinsic exciton absorption of TiO_2, which was observed only with the core–shell structures with the TiO_2 shell.[43] SiO_2@TiO_2 composites show only the TiO_2 absorption edge, whereas core–shell composites containing AuNPs have another broad peak in the visible region, which is attributed to the LSPR band of AuNPs. The observed LSPR band was slightly red-shifted and

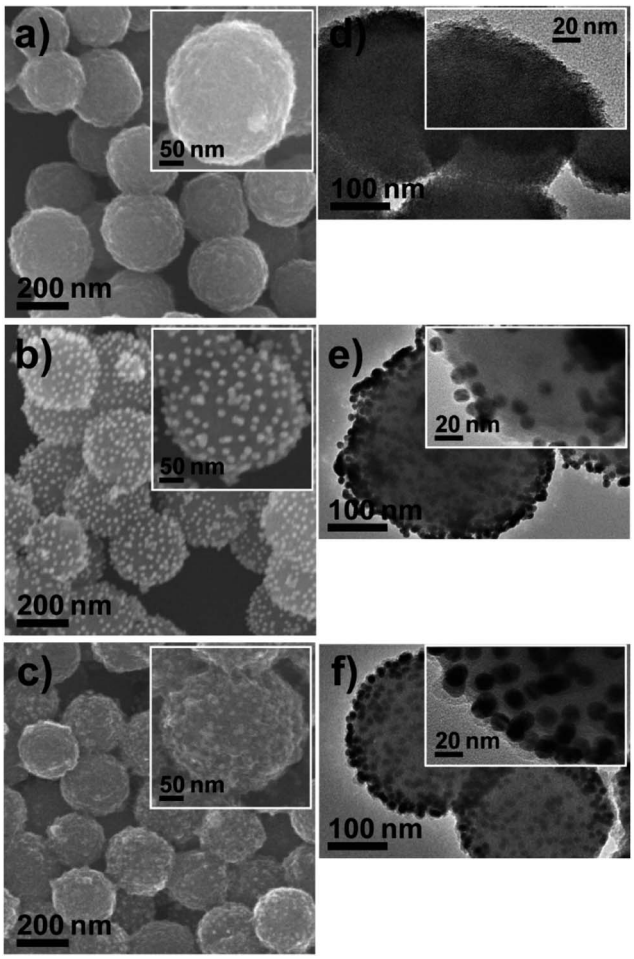

Fig. 1 SEM (left part) and TEM (right part) images of (a and d) SiO_2@TiO_2, (b and e) SiO_2@TiO_2@AuNP, and (c and f) SiO_2@AuNP@TiO_2 core–shell structures. The inset is the corresponding magnified image.

broadened in the core–shell composites relative to that observed from the as-synthesized citrate-capped AuNPs (Fig. S2b†), because LSPR is very sensitive to the index of the surrounding environment.[10] The LSPR wavelengths for AuNPs at the various interfaces were observed as follows: 519 nm for neat AuNP, 526 nm for AuNP at the interface of SiO_2 and outer air (SiO_2@AuNP), 529 nm for AuNP at the interface of TiO_2 and outer air (SiO_2@TiO_2@AuNP), and 538 nm for AuNP at the interface of SiO_2 and TiO_2 (SiO_2@Au@TiO_2). The LSPR band positions observed from the core–shell NPs result from the high refractive index value of the surrounding environments (n = 2.493 for amorphous TiO_2 and n = 1.457 for SiO_2 at 632.8 nm) and are in good agreement with the recent results.[40,41,44,45] It is worth noting that the LSPR characteristic of the core–shell nanocomposites containing AuNPs plays an important role in the DSSC performance: (i) absorption by sensitized dye molecules may be increased by amplifying the near-field intensity when energy matches between incident light and the surface plasmons of AuNPs.[25,34,46,47] (ii) Additional photoexcited electrons induced by the surface plasmons of AuNPs can be transferred to the conduction band of TiO_2. The number of valid charge carriers to enhance the photocurrent would be increased.[48–50]

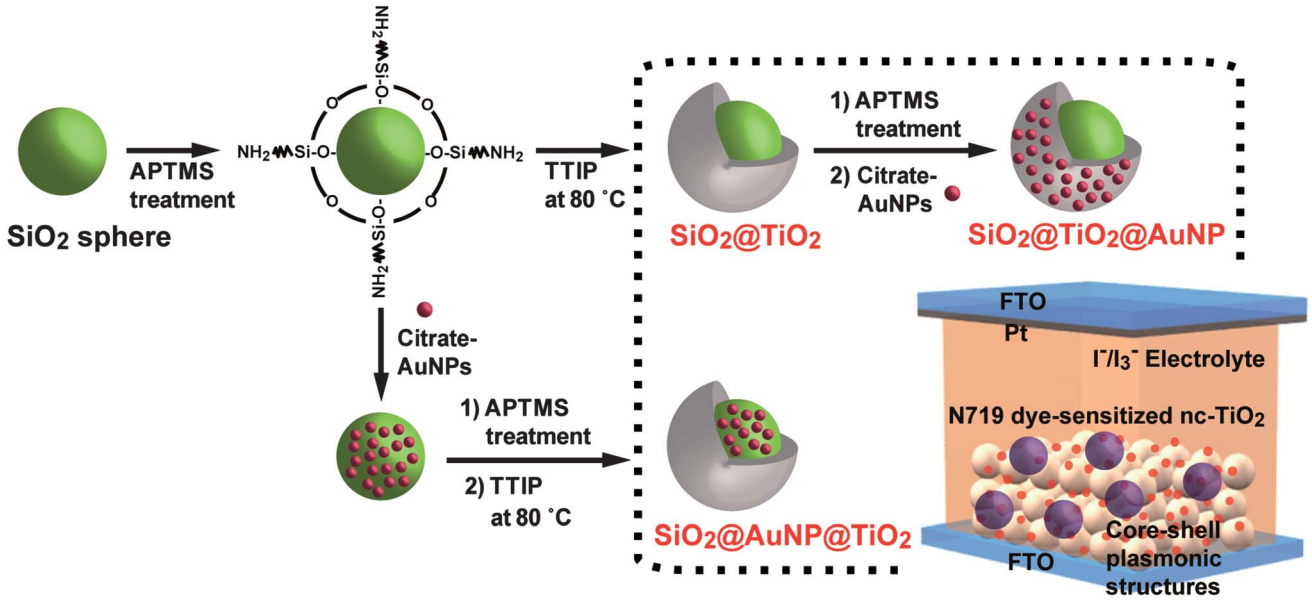

Scheme 1 Schematic illustration of the synthesis process of three types of core–shell photoanode materials (SiO_2@TiO_2, SiO_2@AuNP@TiO_2, and SiO_2@TiO_2@AuNP) for dye-sensitized solar cells.

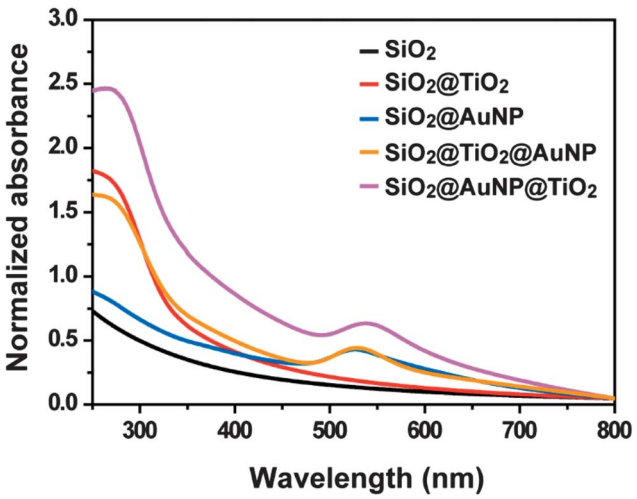

Fig. 2 Normalized UV-Vis absorption spectra of the SiO_2 core, SiO_2@TiO_2, SiO_2@AuNP, SiO_2@TiO_2@AuNP, and SiO_2@AuNP@TiO_2 colloids in aqueous solution. The powder-type samples were dispersed in deionized water for measurement, and the graph presented was normalized with the absorbance value at a wavelength of 800 nm.

The role of the SiO_2 support was examined prior to the investigation of the LSPR effect in plasmonic DSSCs containing tailored AuNPs. The photovoltaic performance of nc-TiO_2 based DSSCs including SiO_2@TiO_2 core–shell structures of different sizes was characterized. The size of SiO_2 spheres was varied by controlling the amount of reactant and catalyst, and the details of the synthesis conditions are summarized in Table S1.†[37] The SiO_2 spheres prepared by the sol–gel process were nearly monodisperse with average sizes of 50 nm, 200 nm, and 400 nm (Fig. S1†). SEM images of the size-controlled SiO_2@TiO_2 core–shell structures are provided in Fig. S4.† As shown in Fig. S4,† thin TiO_2 shells were uniformly formed on the SiO_2 cores, irrespective of the core size. The device was composed of N719 dye-sensitized nc-TiO_2 films (thickness of ~5 μm and active area of ~0.25 cm^2) containing a certain amount of core–shell structure as a photoanode, and a platinum-coated counter electrode. Electrolytes consisting of iodide/triiodide in acetonitrile–valeronitrile were injected in sandwich-typed solar cells. The current–voltage (J–V) responses were recorded under front illumination at an intensity of 100 mA cm^{-2}, and a black mask was applied to the surrounding active area to prevent diffuse light from penetrating into the dye-loaded film through the glass texture. Fig. 3 shows the J–V curves of normal DSSCs as a control (solar cells without core–shell structures) and DSSCs containing size-controlled (50, 200 and 400 nm size) SiO_2@TiO_2 core–shell structures. The loading amount of core–shell structures and thickness of the entire TiO_2 films containing core–shell structures were fixed at 0.5 wt% and 5 μm, respectively. The open-circuit voltage (V_{oc}), short-circuit current density (J_{sc}), fill factor (FF), and overall conversion efficiency (η) are summarized in Table 1. It is found that the SiO_2@TiO_2 core–shell embedded cells exhibit increased efficiency compared to normal DSSCs. The higher efficiency of DSSCs with the size-controlled SiO_2@TiO_2 core–shell structures added was due to the notably increased J_{sc} value from 8.25 mA cm^{-2} for a reference DSSC to 9.94 mA cm^{-2} for a cell including 50 nm SiO_2@TiO_2. The increase in J_{sc} for DCCSs containing SiO_2@TiO_2 particles could be interpreted as an enhanced scattering effect, which allowed the dye to absorb more photons.[51–53] However, with the increasing size of SiO_2, the values of photovoltaic parameters were slightly diminished, which can result from complex factors such as decreased surface area, low reflectance property, and reduced electron transport, *etc.*[53,54]

In order to investigate the mechanism for the plasmonic effects, the performance of DSSCs containing core–shell structures and normal DSSCs was compared. The SiO_2@TiO_2, SiO_2@TiO_2@AuNP, and SiO_2@AuNP@TiO_2 core–shell nanoparticles

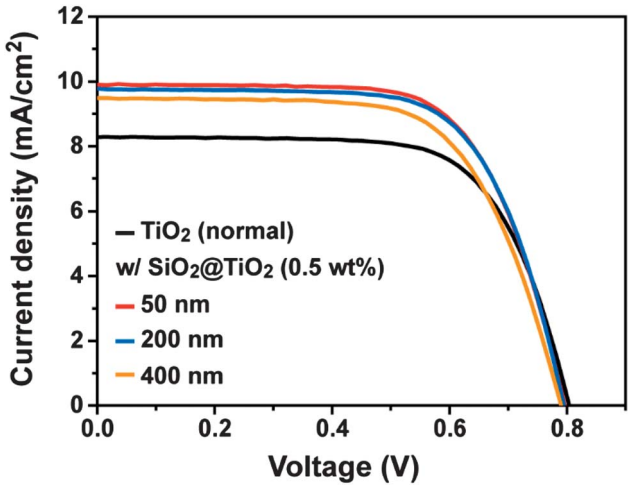

Fig. 3 Photocurrent density–voltage (J–V) curves of normal DSSCs and size-controlled SiO_2@TiO_2 core–shell nanoparticle-containing DSSCs.

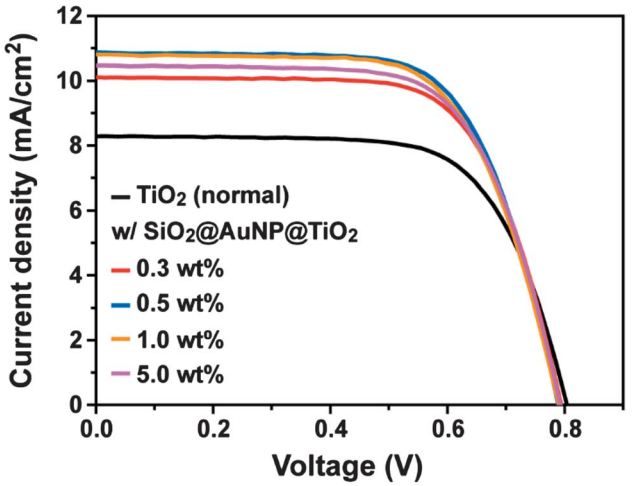

Fig. 4 Photocurrent density–voltage (J–V) curves of normal DSSCs and SiO_2@AuNP@TiO_2 core–shell nanoparticle-containing DSSCs with different concentrations (the size of SiO_2 support is 200 nm).

Table 1 Summary of the photovoltaic parameters of normal DSSCs and size-controlled SiO_2@TiO_2 core–shell nanoparticle-containing DSSCs (the loading amount of core–shell structures is 0.5 wt%)

Sample[a]	V_{oc} (V)	J_{sc} (mA cm^{-2})	FF	PCE (η, %)
Normal	0.803 (±0.002)	8.25 (±0.03)	68.1 (±0.4)	4.51 (±0.05)
50 nm	0.793 (±0.004)	9.94 (±0.04)	66.8 (±0.4)	5.27 (±0.04)
200 nm	0.793 (±0.003)	9.79 (±0.02)	67.4 (±0.2)	5.23 (±0.02)
400 nm	0.788 (±0.003)	9.53 (±0.04)	65.3 (±0.2)	4.90 (±0.01)

[a] Normal DSSCs as a control (without core–shell structures); DSSCs containing size-controlled SiO_2@TiO_2 core–shell nanoparticles. The thickness and active area of films are 5 μm and 0.25 cm^2, respectively. The photovoltaic parameters were recorded under front illumination at an intensity of 100 mA cm^{-2}, and a black mask was applied to the surrounding active area. Average values with standard deviations were obtained from a large number of cells (three cells) for each sample.

were incorporated into normal TiO_2 paste with a fixed SiO_2 core size of 200 nm, and a concentration of 0.5 wt%. To find the optimal concentration of plasmonic core–shell structures, SiO_2@AuNP@TiO_2 core–shell structures with varied concentrations were incorporated into TiO_2. When the concentration was increased from 0.3 wt% to 0.5 wt%, the photocurrent was gradually increased, as shown in Fig. 4 and Table 2. However, when the concentration was increased further, the photocurrent decreased, presumably because the AuNPs act as recombination sites of excited electrons.[30,35,55] Consequently, to maximize the plasmonic effect in DSSCs, the optimal concentration of the plasmonic core–shell structure was decided to be 0.5 wt%.

The SiO_2@TiO_2 core–shell-embedded cell was tested as a reference to investigate the effect of LSPR on the device performance. Fig. 5 shows the J–V curves of plasmon-enhanced DSSCs, and the corresponding photovoltaic parameters are summarized in Table 3. As shown in Fig. 5 and Table 3, the overall conversion efficiency was remarkably improved when plasmonic core–shell structures were included, which was caused by the increase in J_{sc}. Compared with the reference cell employing nc-TiO_2/SiO_2@TiO_2 as the photoanode, the degrees of enhancement in J_{sc} were found to be ~17% and ~11% for plasmon-enhanced cells containing SiO_2@TiO_2@AuNP and SiO_2@AuNP@TiO_2, respectively. It is interesting to note that the SiO_2@TiO_2@AuNP-containing cell shows a higher enhancement ratio in J_{sc} than the SiO_2@AuNP@TiO_2-containing cell, although these two plasmonic core–shell structures differ only regarding the contact between the dye and the AuNPs. Hupp *et al.* previously reported that plasmon-enhanced dye excitation by an electromagnetic field decreased as the distance between dye molecules and plasmonic nanoparticles increased.[25] In the case of SiO_2@AuNP@TiO_2 core–shell structures, AuNPs were effectively protected by the TiO_2 shell from the electrolyte for stability, while the electromagnetic field induced by the AuNPs was shielded. In contrast, in the case of SiO_2@TiO_2@AuNP core–shell structures, AuNPs were exposed to the electrolyte, resulting in slightly low V_{oc} and fill factor, such that the plasmon-enhanced photocurrent should accordingly increase. It is also noted that the chemical stability of decorated AuNPs is

Table 2 Summary of the photovoltaic parameters of normal DSSCs and SiO_2@AuNP@TiO_2 core–shell nanoparticle-containing DSSCs with different concentrations (the size of SiO_2 support is 200 nm)

Sample[a]	V_{oc} (V)	J_{sc} (mA cm^{-2})	FF	PCE (η, %)
Normal	0.803 (±0.002)	8.25 (±0.03)	68.1 (±0.4)	4.51 (±0.05)
0.3 wt%	0.791 (±0.004)	10.13 (±0.03)	68.0 (±0.3)	5.44 (±0.03)
0.5 wt%	0.785 (±0.005)	10.91 (±0.05)	67.0 (±0.4)	5.74 (±0.04)
1.0 wt%	0.786 (±0.005)	10.86 (±0.06)	66.4 (±0.2)	5.66 (±0.02)
5.0 wt%	0.789 (±0.005)	10.51 (±0.05)	67.1 (±0.1)	5.56 (±0.01)

[a] Normal DSSCs as a control (without core–shell structures); DSSCs containing SiO_2@AuNP@TiO_2 core–shell nanoparticles with different concentrations. The thickness and active area of films are 5 μm and 0.25 cm^2, respectively. The photovoltaic parameters were recorded under front illumination at an intensity of 100 mA cm^{-2}, and a black mask was applied to the surrounding active area. Average values with standard deviations were obtained from over a large number of cells (three cells) for each sample.

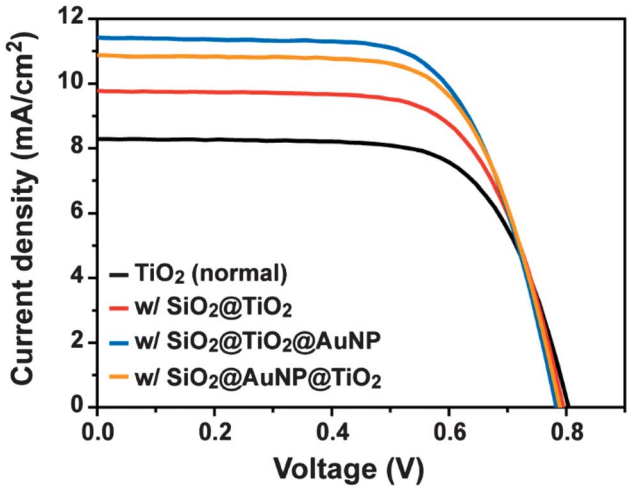

Fig. 5 Photocurrent density–voltage (J–V) curves of normal DSSCs and different types of core–shell nanoparticle-containing DSSCs: (I) SiO_2@TiO_2, (II) SiO_2@TiO_2@AuNP, and (III) SiO_2@AuNP@TiO_2 (the size of SiO_2 support is 200 nm and the loading amount of core–shell structures is 0.5 wt%).

Table 3 Summary of the photovoltaic parameters of normal DSSCs and different types of core–shell nanoparticle-containing DSSCs (the size of the SiO_2 support is 200 nm and the loading amount of core–shell structures is 0.5 wt%)

Sample[a]	V_{oc} (V)	J_{sc} (mA cm^{-2})	FF	PCE (η, %)
Normal	0.803 (±0.002)	8.25 (±0.03)	68.1 (±0.4)	4.51 (±0.05)
I	0.793 (±0.003)	9.79 (±0.02)	67.4 (±0.2)	5.23 (±0.02)
II	0.779 (±0.004)	11.48 (±0.06)	66.4 (±0.3)	5.94 (±0.03)
III	0.785 (±0.005)	10.91 (±0.05)	67.0 (±0.4)	5.74 (±0.04)

[a] Normal DSSCs as a control (without core–shell structures); DSSCs containing different types of core–shell nanoparticles: (I) SiO_2@TiO_2, (II) SiO_2@TiO_2@AuNP, and (III) SiO_2@AuNP@TiO_2. The thickness and active area of films are 5 μm and 0.25 cm^2, respectively. The photovoltaic parameters were recorded under front illumination at an intensity of 100 mA cm^{-2}, and a black mask was applied to the surrounding active area. Average values with standard deviations were obtained from over a large number of cells (three cells) for each sample.

significantly increased due to the adsorbed dyes.[56] Another thing to note is that a slightly decreased V_{oc} was observed in every DSSC with core–shell structures added in comparison to reference DSSCs. There are contradictory reports on the increase[35] or decrease[31] in the V_{oc} value induced by the presence of metal NPs in the photoanode. V_{oc} is typically in proportion to the difference between the quasi-Fermi level and the Nernst potential of the redox couple.[57] Thus, the slight decrease in V_{oc} can be explained by the down-shifted Fermi level due to the incorporation of plasmonic core–shell particles.[31] Furthermore, in the case of the SiO_2@TiO_2@Au loaded cell, a further decrease in V_{oc} as well as fill factor was observed, which may imply that exposed AuNPs can act as recombination centres. In plasmonic solar cells, incorporated metal nanoparticles may have several roles: (i) to increase the light harvesting due to the strong near-field effects of LSPR; (ii) generation of hot electrons by surface plasmon excitation; (iii) to act as electron recombination sites. These factors can competitively have an impact on the device performance.

The enhanced J_{sc} is related to the light harvesting capability of dye molecules by plasmon-enhanced excitation. Fig. 6a shows the UV-Vis absorption spectra of nc-TiO_2 films containing core–shell structures before (solid line) and after (dotted line) dye loading on the FTO substrate. The broad and weak LSPR bands of decorated AuNPs in the plasmonic anode appeared in the range of 500–600 nm with a peak center around 550 nm (indicated by the upward arrow in Fig. 6a), which differ from the characteristic bands of isolated core–shell structures due to the existence of the nc-TiO_2 particles surrounding the core–shell structures. The absorption band of N719 dye was also observed around 380 and 530 nm (indicated by the downward arrows in Fig. 6a), and the optical absorption enhancement was observed in the dye-loaded plasmonic core–shell composite-embedded films. The relative changes in optical absorption (ΔOA/OA) of the dye molecules in SiO_2@TiO_2@AuNP and SiO_2@AuNP@TiO_2 embedded films are shown in Fig. 6b. The relatively broad and strong enhancement is observed in the range of 500–600 nm with a maximum enhancement around 550 nm, which coincides with the LSPR band position of decorated AuNPs (Fig. 6a). These features suggest that dye molecules in the vicinity of AuNPs can absorb more photons, presumably due to the intensified near-field effect of the surface plasmon and spectral overlap between the dye and surface plasmon, which may eventually lead to an increase in the number of charge carriers and J_{sc} values.

In order to investigate the spectral response of plasmon-enhanced DSSCs, incident photon-to-current efficiency (IPCE) measurement was performed. As shown in Fig. 7a, IPCE spectra were analogous to an absorption spectrum of N719 dye molecules (grey line) and the plasmon-enhanced devices containing plasmonic core–shell structures (SiO_2@TiO_2@AuNP and SiO_2@AuNP@TiO_2) exhibit higher IPCE than the device containing the SiO_2@TiO_2 core–shell structure over the whole wavelength ranges. Fig. 7b shows the IPCE enhancement ratio (ΔIPCE/IPCE, %) of plasmon-enhanced DSSCs with SiO_2@TiO_2@AuNPs or SiO_2@AuNP@TiO_2 core–shell structures added with respect to DSSCs with SiO_2@TiO_2 core–shell structures added. It is found that the IPCE enhancement is observed over a broad spectral range rather than around the LSPR band of plasmonic nanostructures. The increase observed at the lower and mid wavelength region can be interpreted by two mechanisms: (i) increased dye excitation arising from the enhanced near-field effects of AuNPs: to verify plasmon-enhanced dye excitation, concentrations of dye molecules on each photoanode were calculated from UV-Vis spectra of desorbed dye molecules using 0.2 M NaOH solution. The amounts of desorbed dye were 9.62×10^{-5} mmol cm^{-2} for the normal TiO_2 photoanode and 9.73×10^{-5}, 9.57×10^{-5}, and 8.63×10^{-5} mmol cm^{-2} for photoanodes containing SiO_2@TiO_2 (I), SiO_2@TiO_2@AuNP (II), and SiO_2@AuNP@TiO_2 (III), respectively. The dye coverage was similar to each other, which proves that increased IPCE is caused by near-field effects of AuNPs. (ii) Contribution of the transfer of plasmon-induced excited hot electrons to the conduction band of TiO_2 (refer to more

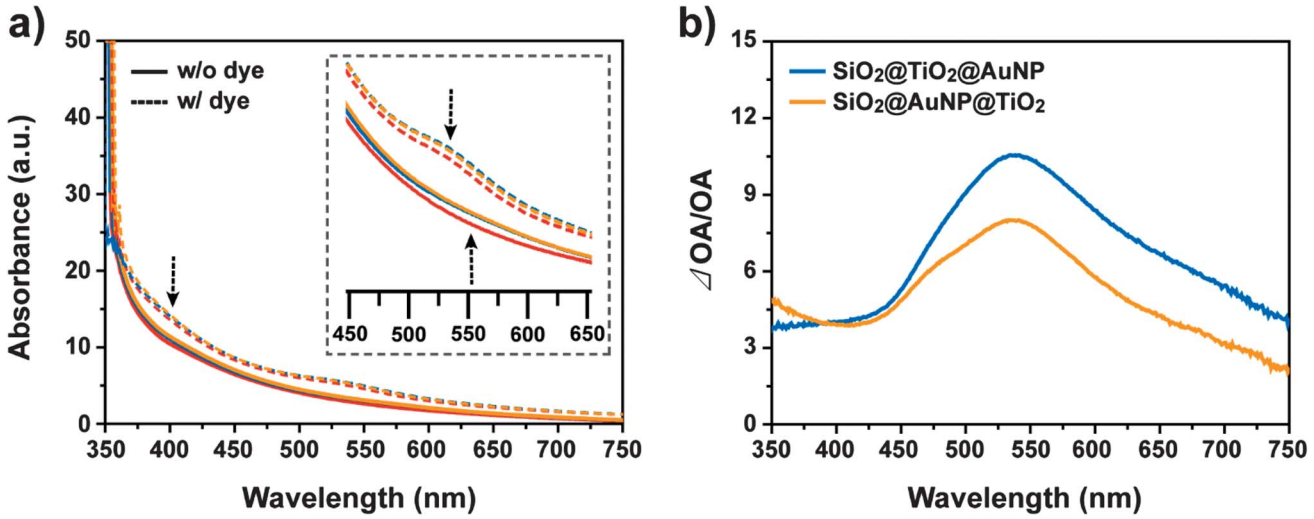

Fig. 6 (a) UV-Vis absorption spectra of three different photoanode films on an FTO substrate (a) without (solid line) and with dye (dotted line) molecules: nc-TiO_2/SiO_2@TiO_2 (red line), nc-TiO_2/SiO_2@TiO_2@AuNP (blue line), nc-TiO_2/SiO_2@AuNP@TiO_2 (orange line) (the size of SiO_2 support is 200 nm and the loading amount of core–shell structures is 0.5 wt%). (b) Relative changes in optical absorption (ΔOA/OA) of dye molecules in the plasmonic anode, SiO_2@TiO_2@AuNP and SiO_2@AuNP@TiO_2 embedded films. $\Delta OA/OA = (Abs._{nc\text{-}TiO_2/SiO_2@TiO_2@AuNP\ (or\ SiO_2@AuNP@TiO_2)+dye}(\lambda) - Abs._{nc\text{-}TiO_2/SiO_2@TiO_2+dye}(\lambda))/(Abs._{nc\text{-}TiO_2/SiO_2@TiO_2+dye}(\lambda)) \times 100$.

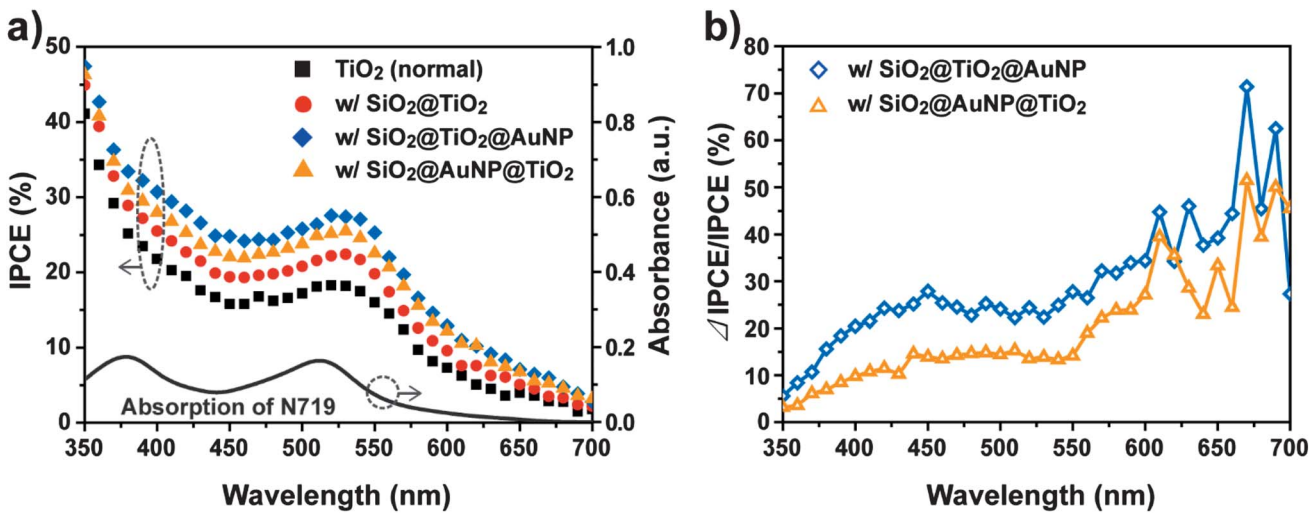

Fig. 7 (a) Incident photon-to-current conversion efficiency (IPCE) curves of normal DSSCs and DSSCs composed of nc-TiO_2/SiO_2@TiO_2, nc-TiO_2/SiO_2@TiO_2@AuNP, and nc-TiO_2@SiO_2@AuNP@TiO_2 as photoanodes (the size of SiO_2 support is 200 nm and the loading amount of core–shell structures is 0.5 wt%). (b) IPCE enhancement ratio (ΔIPCE/IPCE, %) of plasmon-enhanced DSSCs with core–shell structures. $\Delta IPCE/IPCE\ (\%) = (IPCE_{DSSCs\ with\ SiO_2@TiO_2@AuNP\ (or\ SiO_2@AuNP@TiO_2)}(\lambda) - IPCE_{DSSCs\ with\ SiO_2@TiO_2}(\lambda))/(IPCE_{DSSCs\ with\ SiO_2@TiO_2}(\lambda)) \times 100\ (\%)$.

discussion in the following section).[49,50,58] The enhancement ratio increase at longer wavelength could be a manifestation of the poor signal-to-noise ratio in this spectral region.

To provide the evidence on increased photocurrent by plasmon-assisted photocurrent generation in AuNPs, photoelectrochemical measurement was performed using a three-electrode system through linear-sweep voltammetry (LSV). The core–shell structure-containing TiO_2 films without dye molecules on the FTO substrate, Pt plate, and the Ag/AgCl electrode in 3 M KCl were used as the working electrode, counter electrode, and reference electrode, respectively. Fig. 8 shows the photocurrent *versus* potential curves measured under visible light irradiation (using a cut-off filter with a wavelength of 420 nm) in 0.1 M NaOH electrolyte. As shown in Fig. 8, an anodic photocurrent was observed for the plasmonic core–shell structure-containing films, as well as the normal TiO_2 film. A negligible difference is observed in the photoanodic curves between the normal TiO_2 film and the SiO_2@TiO_2-containing film, while the plasmonic core–shell structure-containing films show increased photocurrent values even if stability is not guaranteed after five-more-sweeps (Fig. S5†). This is probably due to plasmonic-induced photocurrents, in that the hot electrons driven from the surface plasmon-induced charge separation of AuNPs can be injected into the conduction band of TiO_2, resulting in plasmon-assisted

photocurrent generation. The plasmonically excited electron extraction from metals to TiO_2 semiconductors has been experimentally and theoretically studied in previous reports.[59–62] However, the exact mechanism for the surface plasmon-induced charge separation process in plasmonic photovoltaic devices is not clarified yet. Reineck *et al.* proposed a few possible mechanisms for plasmon-induced charge separation in a plasmonic solar cell system:[50] (i) both hot electrons and holes resulting from the excitation of surface plasmon can be concurrently injected into the TiO_2 conduction band and solid state electrolyte, respectively, which would occur on femtosecond timescale. (ii) One type of the hot charge carriers, *i.e.*, excited electron–hole pairs, can be transferred and the opposite charge accumulation would lead to Fermi level shift to the point where it can thermally transfer to either the TiO_2 conduction band or the solid state electrolyte. Based on these assumptions, we can conjecture that plasmon-induced hot electrons can be transferred into the TiO_2 conduction band, while remaining hot holes can be injected into electrolyte media, leading to facile separation of the hot charge carriers. To demonstrate the charge separation of plasmon-induced hot carriers, photocurrent response to the visible light illumination was measured through the photoelectrochemical water splitting system. For this experiment, SiO_2@TiO_2 and SiO_2@TiO_2@AuNP core–shell structures were deposited on the ITO substrate and used as the working electrode. Pt plate and Ag/AgCl were used as the counter electrode and reference electrode, respectively. As shown in Fig. S6,† SiO_2@TiO_2@AuNP could effectively harness visible light photon and exhibit photocurrent generation. Without Au nanoparticles, however, SiO_2@TiO_2 does not respond to visible light excitation. Furthermore, to investigate the contribution of photons with a specific wavelength to plasmonically enhanced charge extraction, the monochromatic laser of 532 nm with 10 mW power (refer to the plasmon resonance wavelength of the AuNP-decorated core–shell nanostructures close to 532 nm wavelength in Fig. 2) was illuminated.[62] The photoelectrocatalytic activity under the 532 nm monochromatic illumination was examined using cyclic voltammetry (CV) in oxygen-saturated 0.1 M KOH. The SiO_2@TiO_2@AuNP core–shell structure shows conspicuously increased photocurrent than the AuNP-free sample. The resulting photocurrent could be assigned to the photo-oxidation by plasmon-induced hot holes.

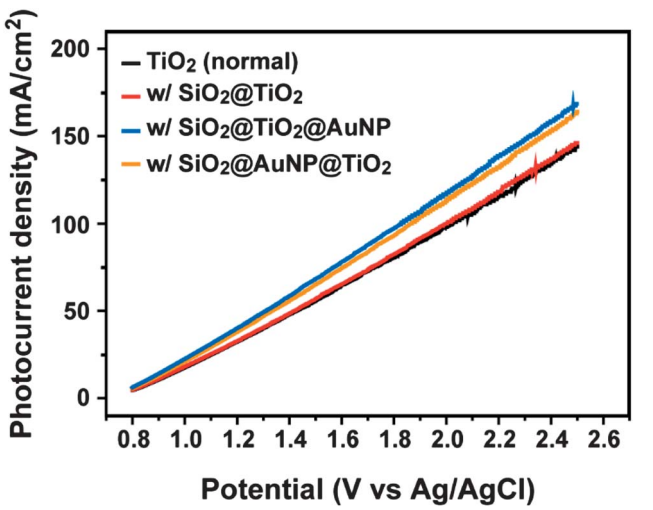

Fig. 8 Photocurrent *versus* potential characteristics (linear-sweep voltammetry, LSV curves) of the normal TiO_2 film and SiO_2@TiO_2, SiO_2@TiO_2@AuNP, and SiO_2@AuNP@TiO_2-containing TiO_2 films in 0.1 M NaOH electrolyte under visible light illumination (the size of SiO_2 support is 200 nm and the loading amount of core–shell structures is 0.5 wt%).

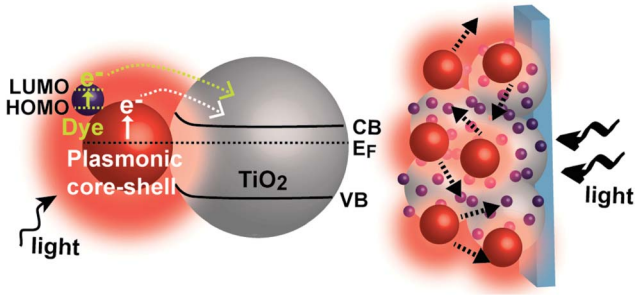

Scheme 2 Schematic illustration representing the increased photocurrent by LSPR and scattering effects.

We conclude that the improved current density may be attributed to not only the increase in the dye excitation by the effects of LSPR associated with near-filed enhancement and scattering, but also to the generation of additional photocurrent owing to the LSPR-induced direct hot-electron transfer from plasmonic core–shell structures to TiO_2 conduction bands (Scheme 2).

Conclusions

In summary, in order to demonstrate the effects of LSPR in DSSCs, we constructed plasmonic DSSCs utilizing tailor-designed SiO_2@TiO_2@AuNP and SiO_2@AuNP@TiO_2 core–shell structures as photoanode additives. The DSSCs employing nc-TiO_2/SiO_2@TiO_2@AuNP and nc-TiO_2/SiO_2@AuNP@TiO_2 as photoanodes showed remarkably enhanced power conversion efficiencies up to about 14% and 10%, respectively, with respect to a reference cell containing an nc-TiO_2/SiO_2@TiO_2 photoanode. Although only a small fraction of plasmonic core–shell structures was introduced, such marked enhancement suggests that LSPR features could affect the cell performance, as well as the strong scattering effects: (1) the intensified near-field of AuNPs can act as antennas for increasing the dye absorption, thereby possibly enhancing J_{sc}; (2) plasmon-assisted photocurrent generation can also contribute to the increase in current density. It is especially worth noting that the DSSCs containing nc-TiO_2 films combined with 0.5 wt% SiO_2@TiO_2@AuNP show superior cell performance to those containing SiO_2@AuNP@TiO_2, owing to the dye excitation enhanced the by the strong electromagnetic field effect from LSPR. It is found that the distance between dye molecules and decorated AuNPs affects the plasmon-enhanced dye excitation. The current study demonstrates a promising route to maximize the performance of plasmonic DSSCs *via* the rational design of tailored plasmonic nanostructures.

Acknowledgements

This work was supported by the National Research Foundation of Korea Grant, funded by the Korean Government (2011-0029409; 2011-0030255). The authors thank Prof. Kyungkon Kim at Ewha Womans University for IPCE measurements.

Notes and references

1 A. N. Shipway, E. Katz and I. Willner, *ChemPhysChem*, 2000, **1**, 18.
2 J. Chen, F. Saeki, B. J. Wiley, H. Cang, M. J. Cobb, Z.-Y. Li, L. Au, H. Zhang, M. B. Kimmey, X. Li and Y. Xia, *Nano Lett.*, 2005, **5**, 473.
3 S. M. Borisov and O. S. Wolfbeis, *Chem. Rev.*, 2008, **108**, 423.
4 J. E. Lee, K. Chung, Y. H. Jang, Y. J. Jang, S. T. Kochuveedu, D. X. Li and D. H. Kim, *Anal. Chem.*, 2012, **84**, 6494.
5 P. V. Kamat, *J. Phys. Chem. B*, 2002, **106**, 7729.
6 V. Subramanian, E. E. Wolf and P. V. Kamat, *J. Am. Chem. Soc.*, 2004, **126**, 4943.
7 S. Nie and S. R. Emory, *Science*, 1997, **275**, 1102.
8 A. M. Michaels, J. Jiang and L. Brus, *J. Phys. Chem. B*, 2000, **104**, 11965.
9 Y. Fang, N. H. Seong and D. D. Dlott, *Science*, 2008, **321**, 388.
10 K. L. Kelly, E. Coronado, L. L. Zhao and G. C. Schatz, *J. Phys. Chem. B*, 2003, **107**, 668.
11 E. Hutter and J. H. Fendler, *Adv. Mater.*, 2004, **16**, 1685.
12 S. Eustis and M. A. El-Sayed, *Chem. Soc. Rev.*, 2006, **35**, 209.
13 K. A. Willets and R. P. Van Duyne, *Annu. Rev. Phys. Chem.*, 2007, **58**, 267.
14 K. Catchpole and A. Polman, *Opt. Express*, 2008, **16**, 21793.
15 C. Hägglund and B. Kasemo, *Opt. Express*, 2009, **17**, 11944.
16 V. E. Ferry, J. N. Munday and H. A. Atwater, *Adv. Mater.*, 2010, **22**, 4794.
17 H. A. Atwater and A. Polman, *Nat. Mater.*, 2010, **9**, 205.
18 S. Pillai and M. Green, *Sol. Energy Mater. Sol. Cells*, 2010, **94**, 1481.
19 I. Thomann, B. A. Pinaud, Z. Chen, B. M. Clemens, T. F. Jaramillo and M. L. Brongersma, *Nano Lett.*, 2011, **11**, 3440.
20 M. A. Green and S. Pillai, *Nat. Photonics*, 2012, **6**, 130.
21 D. Derkacs, S. Lim, P. Matheu, W. Mar and E. Yu, *Appl. Phys. Lett.*, 2006, **89**, 093103.
22 K. Nakayama, K. Tanabe and H. A. Atwater, *Appl. Phys. Lett.*, 2008, **93**, 121904.
23 J. You, X. Li, F. Xie, W. E. I. Sha, J. H. W. Kwong, G. Li, W. C. H. Choy and Y. Yang, *Adv. Eng. Mater.*, 2012, **2**, 1203.
24 D. H. Wang, K. H. Park, J. H. Seo, J. Seifter, J. H. Jeon, J. K. Kim, J. H. Park, O. O. Park and A. J. Heeger, *Adv. Eng. Mater.*, 2011, **1**, 766.
25 S. D. Standridge, G. C. Schatz and J. T. Hupp, *J. Am. Chem. Soc.*, 2009, **131**, 8407.
26 G. Zhao, H. Kozuka and T. Yoko, *Sol. Energy Mater. Sol. Cells*, 1997, **46**, 219.
27 M. Ihara, K. Tanaka, K. Sakaki, I. Honma and K. Yamada, *J. Phys. Chem. B*, 1997, **101**, 5153.
28 C. Wen, K. Ishikawa, M. Kishima and K. Yamada, *Sol. Energy Mater. Sol. Cells*, 2000, **61**, 339.
29 C. Hagglund, M. Zach and B. Kasemo, *Appl. Phys. Lett.*, 2008, **92**, 013113.
30 J. Qi, X. Dang, P. T. Hammond and A. M. Belcher, *ACS Nano*, 2011, **5**, 7108.
31 J. Du, J. Qi, D. Wang and Z. Tang, *Energy Environ. Sci.*, 2012, **5**, 6914.
32 G. Sahu, S. W. Gordon and M. A. Tarr, *RSC Adv.*, 2012, **2**, 573.
33 S. Chang, Q. Li, X. Xiao, Y. K. Wong and T. Chen, *Energy Environ. Sci.*, 2012, **5**, 9444.
34 M. D. Brown, T. Suteewong, R. S. S. Kumar, V. D'Innocenzo, A. Petrozza, M. M. Lee, U. Wiesner and H. J. Snaith, *Nano Lett.*, 2011, **11**, 438.
35 H. Choi, W. T. Chen and P. V. Kamat, *ACS Nano*, 2012, **6**, 4418.
36 W. Stöber, A. Fink and E. Bohn, *J. Colloid Interface Sci.*, 1968, **26**, 62.
37 J. Kim, L. Kim and C. Kim, *Biomacromolecules*, 2007, **8**, 215.
38 J. Turkevich, P. C. Stevenson and J. Hillier, *Discuss. Faraday Soc.*, 1951, **11**, 55.
39 Y. H. Jang, X. Xin, M. Byun, Y. J. Jang, Z. Lin and D. H. Kim, *Nano Lett.*, 2011, **12**, 479.
40 S. T. Kochuveedu, D.-P. Kim and D. H. Kim, *J. Phys. Chem. C*, 2012, **116**, 2500.
41 Q. Zhang, D. Q. Lima, I. Lee, F. Zaera, M. Chi and Y. Yin, *Angew. Chem., Int. Ed.*, 2011, **123**, 7226.
42 L. You, Y. Mao and J. Ge, *J. Phys. Chem. C*, 2012, **116**, 10753.
43 A. L. Linsebigler, G. Lu and J. T. Yates Jr, *Chem. Rev.*, 1995, **95**, 735.
44 J. R. DeVore, *J. Opt. Soc. Am.*, 1951, **41**, 416.
45 I. Malitson, *J. Opt. Soc. Am.*, 1965, **55**, 1205.
46 C. Nahm, H. Choi, J. Kim, D.-R. Jung, C. Kim, J. Moon, B. Lee and B. Park, *Appl. Phys. Lett.*, 2011, **99**, 253107.
47 S. D. Standridge, G. C. Schatz and J. T. Hupp, *Langmuir*, 2009, **25**, 2596.
48 Y. Tian and T. Tatsuma, *J. Am. Chem. Soc.*, 2005, **127**, 7632.
49 S. Mubeen, J. Lee, N. Singh, S. Krämer, G. D. Stucky and M. Moskovits, *Nat. Nanotechnol.*, 2013, **8**, 247.
50 P. Reineck, G. P. Lee, D. Brick, M. Karg, P. Mulvaney and U. Bach, *Adv. Mater.*, 2012, **24**, 4750.
51 Z.-S. Wang, H. Kawauchi, T. Kashima and H. Arakawa, *Coord. Chem. Rev.*, 2004, **248**, 1381.
52 F. Huang, D. Chen, X. L. Zhang, R. A. Caruso and Y. B. Cheng, *Adv. Funct. Mater.*, 2010, **20**, 1301.
53 H.-J. Koo, J. Park, B. Yoo, K. Yoo, K. Kim and N.-G. Park, *Inorg. Chim. Acta*, 2008, **361**, 677.
54 Z.-S. Wang, H. Kawauchi, T. Kashima and H. Arakawa, *Coord. Chem. Rev.*, 2004, **248**, 1381.
55 Q. Xu, F. Liu, Y. Liu, K. Cui, X. Feng, W. Zhang and Y. Huang, *Sci. Rep.*, 2013, **3**, 2112.

56 B. Ding, B. J. Lee, M. Yang, H. S. Jung and J. K. Lee, *Adv. Eng. Mater.*, 2011, **1**, 415.
57 B. O'Regan and M. Grätzel, *Nature*, 1991, **353**, 737.
58 Y. Nishijima, K. Ueno, Y. Yokota, K. Murakoshi and H. Misawa, *J. Phys. Chem. Lett.*, 2010, **1**, 2031.
59 M. W. Knight, H. Sobhani, P. Nordlander and N. J. Halas, *Science*, 2011, **332**, 702.
60 S. Mubeen, G. Hernandez-Sosa, D. Moses, J. Lee and M. Moskovits, *Nano Lett.*, 2011, **11**, 5548.
61 J. Lee, S. Mubeen, X. Ji, G. D. Stucky and M. Moskovits, *Nano Lett.*, 2012, **12**, 5014.
62 D. Zhang, W. C. Choy, F. Xie, W. E. Sha, X. Li, B. Ding, K. Zhang, F. Huang and Y. Cao, *Adv. Funct. Mater.*, 2013, **23**, 4255.